Granular Matter (2013) 15:95–108
DOI 10.1007/s10035-012-0380-x

ORIGINAL PAPER

Generating realistic 3D sand particles using Fourier descriptors

Guilhem Mollon · Jidong Zhao

Received: 1 August 2012 / Published online: 30 October 2012

Abstract This paper presents a novel method of generation of random realistic sand grains for use in three dimensional (3D) DEM simulations. Based on the concept of Fourier descriptors for sand grains proposed recently by the same authors, we first randomly generate three 2D contours of cross-section for a real sand particle in three orthogonal planes, and then develop a morphing technique to construct the external 3D surface of the particle to match these cross-sections. The proposed method is examined by application to the generation of six sands reported in the literature using the Fourier spectrums available for these sands. We show that with a proper correction on the smoothness and roundness of the orthogonal projection calibrated from the six sands, the method can generate fairly consistent results as compared to the real sands. Further validation of the proposed method on another three sands shows satisfactory performance. The advantages and limitations of the method, as well as relevant future applications of the work to granular material modelling are discussed.

Keywords Granular media · 3D particle shape · Fourier descriptors · 3D morphing technique · DEM

1 Introduction

Accurate characterization of the shape of cohesionless particles is pivotal to gain better understanding towards the complex behavior of granular materials for many scientific and industrial applications, such as civil and geotechnical engineering, powders and pharmaceutical industries, mining and energy industry as well as geophysics. Particle shape may affect considerably both the mechanical behavior (such as friction, dilatancy and strength) and the flow behavior (e.g., jamming transition, avalanche and pattern formation) of a granular medium. The interlocking observed in granular sand, for example, has been considered primarily attributable to irregular particle shape and particle angularity, and is closely related to the dilatancy and strength of sand [1,2]. The packing of complex-shaped particles is also of primary interest in the research of nanoparticles and colloïds [3].

Recent granular physics and granular mechanics research has witnessed an increasing interest in using discrete numerical modeling approaches. In particular, the Discrete Element Method (DEM) pioneered by Cundall and Strack [4] has been particularly popular for many researchers. Early studies by DEM have considered circular or spherical particles, due mainly to the great simplicity and computational efficiency it may offer. More recent investigations, however, reveal the profound influence of particle shape on the simulation results in DEM modeling which cannot otherwise be captured by using circular/spherical particles. A variety of different attempts have hence been made to consider particle of more complex shapes, exemplified by using clumps or clusters of discs/spheres [5–11] polygons [12], polyhedrons, sphero-polygons [13] or sphero-polyhedrons [14–22], or ellipses and ellipsoids [23–27] among others. As compared to the circular/spherical case, the consideration of complex particle shapes in DEM simulation has been shown to capture the behavior of granular media better in many aspects, including the packing density [14], shear strength [5,9,14,21], fabric anisotropy [15,24], shear banding and critical state [27] and the reproduction of observation on chute flow [11] and

G. Mollon (✉) · J. Zhao
Department of Civil and Environmental Engineering,
Hong Kong University of Science and Technology,
Clearwater Bay, Kowloon, Hong Kong
e-mail: guilhem.mollon@gmail.com

J. Zhao
e-mail: jzhao@ust.hk

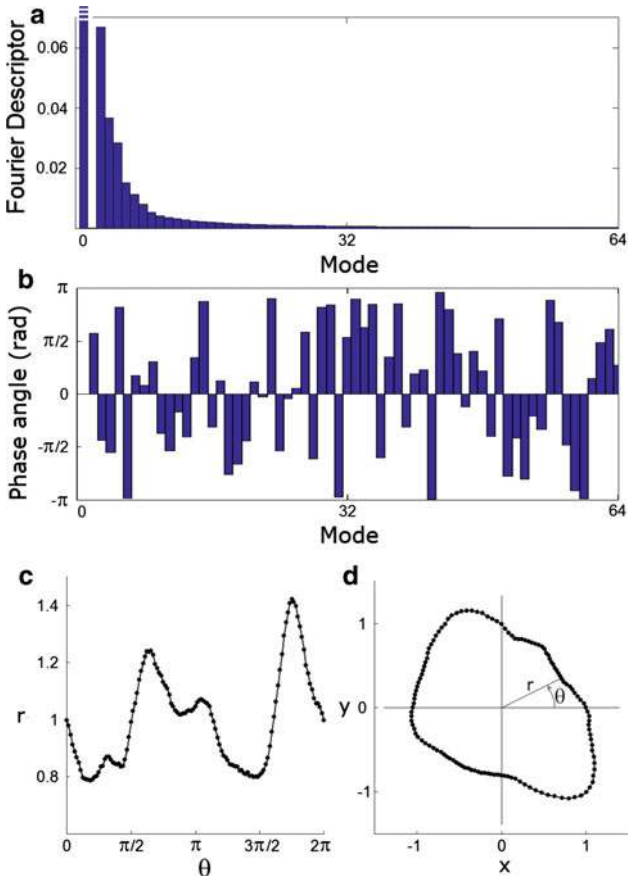

Fig. 1 **a** Illustrative discrete Fourier spectrum; **b** random sampling of phase angles; **c** corresponding r(θ) discrete signal; **d** particle contour in a Cartesian frame

rock avalanche [18,19]. However, the choice of particle shape in the different studies mentioned above has been rather arbitrary. At best they can be regarded limited improvements over the simple sphere/circle approximation in modeling the real particle shape qualitatively. It is more desirable to develop a systematic approach to identify the quantitative information that differentiates the unique particle shape characteristics of one material from the other, and to provide faithful reference for generating more realistic packing of a granular material for DEM simulation. In this paper, we present a general method aiming at generating a random population of particles with some prescribed features reproducing the target real granular material. This method is a 3D extension of a recent 2D framework proposed by the authors [28] based on the concept of Fourier Descriptors. In essence, this method features the reproduction of three cross-sections of a realistic 3D particle using the 2D approach proposed in [28], and then combines these cross-sections to generate the external surface of the particle. As will be shown, the proposed method is robust and efficient in reproducing the salient features that represent a realistic granular particle. It hence offers a possible way for more realistic DEM modeling of granular media.

2 Brief introduction of the 2D Fourier approach

Fourier Descriptors were first introduced in [29] for particle shape characterization, and were further applied by several authors to sand characterization [30–33]. It was shown in these studies that the average normalized Fourier spectrum of the 2D contours (obtained by projection) of a population of particles may embody a relevant signature of the shape features of these particles. Specifically, the normalized Fourier spectrum of a 2D contour for a particle is denoted by a collection of numbers, also called Fourier descriptors:

$$D_n = \frac{\sqrt{A_n^2 + B_n^2}}{r_0} \; (0 \leq n \leq N/2) \tag{1}$$

where the terms A_n, B_n and r_0 can be obtained by Discrete Fourier Transform of the contour expressed in polar (r, θ) coordinates and discretized in N points:

$$A_n = \frac{1}{N} \sum_{i=1}^{N} [r_i \cos(i \cdot \theta_i)] \tag{2}$$

$$B_n = \frac{1}{N} \sum_{i=1}^{N} [r_i \sin(i \cdot \theta_i)] \tag{3}$$

$$r_0 = \frac{1}{N} \sum_{i=1}^{N} [r_i] \tag{4}$$

The normalization (division by r_0) ensures that the mode D_0 (average particle radius) is equal to 1, and a proper choice of the particle centre ensures that the mode D_1 (corresponding to some shift of the particle from its centre) is equal to 0. An example of Fourier Spectrum with $N/2 = 64$ is provided in Fig. 1a. A given particle can be reconstructed from the two collections of numbers, A_n and B_n, as a sum of individual modes, via the following expression:

$$r_i(\theta_i) = r_0 + \sum_{n=1}^{N} [A_n \cos(n\theta) + B_n \sin(n\theta)] \tag{5}$$

This method has been widely used for the characterization of sand particle shapes, since there is a direct correlation between the normalized Fourier spectrum $\{D_\mathrm{n}\}$ and some intrinsic properties of the grains. It was indeed shown that the mode D_2 controls the particle elongation, the modes D_3 to D_7 control the main irregularities of the overall particle shape, and the modes D_n for $n > 7$ (which most often follow a linear decrease with n in a log-log frame and can thus be described using only a slope and an intercept) are good descriptors of the particle surface roughness. Das [33] used this approach to derive the average normalized Fourier spectrums for six sands based on the microscope pictures of a sufficient number of grains of each sand.

Novel to the approach developed by Mollon and Zhao [28] is the employment of the normalized Fourier spectrum

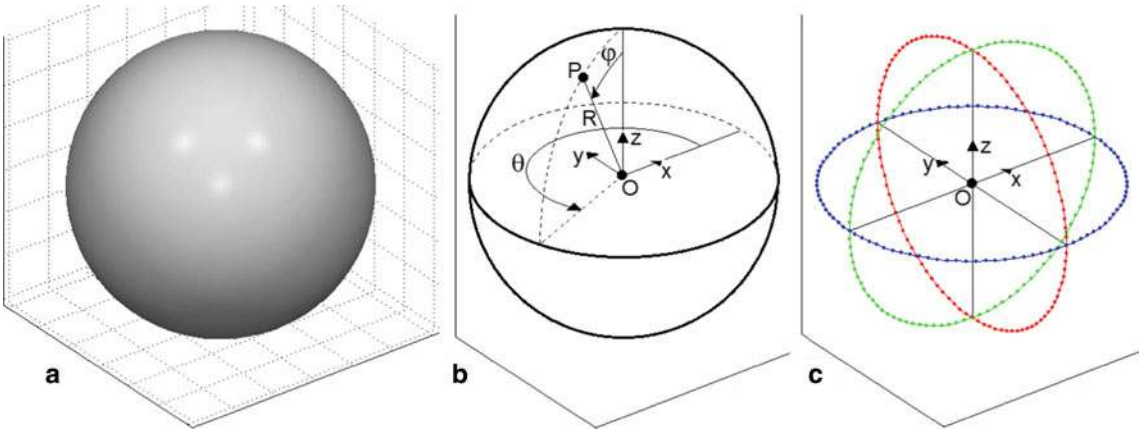

Fig. 2 **a** Unit sphere; **b** description of this sphere in spherical and Cartesian coordinates; **c** cross-sections in three orthogonal planes

as a tool to perform the reverse operation, i.e. to generate random grains with prescribed shape features. As can be seen from Eq. (5), the Fourier Descriptors $\{D_n\}$ by themselves are not sufficient to generate a grain contour, since a part of the information on the initial contour is lost in Eq. (1). More precisely, the lost information is the phase angle of each mode n, expressed by:

$$\delta_n = \tan^{-1}\left(\frac{B_n}{A_n}\right) \tag{6}$$

Thus, a random particle with a prescribed amplitude spectrum $\{D_n\}$ can be generated by randomly assigning a phase angle δ_n to each mode of order greater than one. Each of these random angles is supposed to follow a uniform distribution on the interval $[-\pi\,;\pi]$. The discretized contour of the considered particle is obtained using Eq. (5) by:

$$A_n = D_n \cdot \cos\delta_n \tag{7}$$

$$B_n = D_n \cdot \sin\delta_n \tag{8}$$

The generation of a typical 2D grain with the above Fourier spectrum method is illustrated in Fig. 1. The study reported in [28] has provided several examples of such generations as well as relevant correspondences between the Fourier descriptors and some more common shape descriptors (such as elongation, roundness, circularity, regularity). A fully working version of the MATLAB code of this 2D method is available for free download at the url http://guilhem.mollon.free.fr.

3 Extension of the Fourier approach to the 3D case

3.1 Numerical manipulation of 3D shapes

It is instructive to show how the 3D shapes of a sand grain may be handled numerically. Let us consider the unit sphere of Fig. 2a. The position of a point P at the surface of this sphere can be defined in two classical ways (Fig. 2b), i.e. by either using the Cartesian system of axis (O, x, y, z) or using the spherical system of axis (O, R, θ, φ), where the two approaches can be interchangeable via:

$$\begin{cases} x = R \cdot \cos\theta \cdot \sin\varphi \\ y = R \cdot \sin\theta \cdot \sin\varphi \\ z = R \cdot \cos\varphi \end{cases} \tag{9}$$

When dealing with a sphere, the distance $OP = R$ is constant. In this paper, we will only deal with 3D shapes delimited by closed surfaces such that, for a given direction (θ, φ), there is only one value of R. Such shapes are called "star-like" shapes in [32]. Although there are a few exceptions (such as the crushed shells mentioned in [34]), it is generally believed that star-like shapes are capable of describing the majority of natural geomaterials. Thus, in this framework, a shape will be entirely defined by a continuous function $R(\theta, \varphi)$ with $0 \leq \theta \leq 2\pi$ and $0 \leq \varphi \leq \pi$. However, manipulating such a continuous function in a numerical environment is not easy where a discretization of these surfaces is frequently required. One may elect to discretize each angular coordinate θ and φ in equal intervals. This approach however is not recommended since it may result in uneven distribution of the discretized points on the shape surface (more specifically, there would be a much larger density of points at the poles than at the equator). We herein choose an alternative approach based on the concept of geodesic structures which are widely used in architecture, as shown in Fig. 3. These structures allow a rather even discretization of the surface of a sphere with a large number of triangular facets. A simple way to generate such a structure is to consider the icosahedron (Fig. 3a), which is also known as the fifth Platonic solid. This classical shape is composed of 20 triangular faces and 12 vertices which all belong to the circumscribed sphere of the solid. A more complex geodesic structure can be generated from the icosahedron in a rather

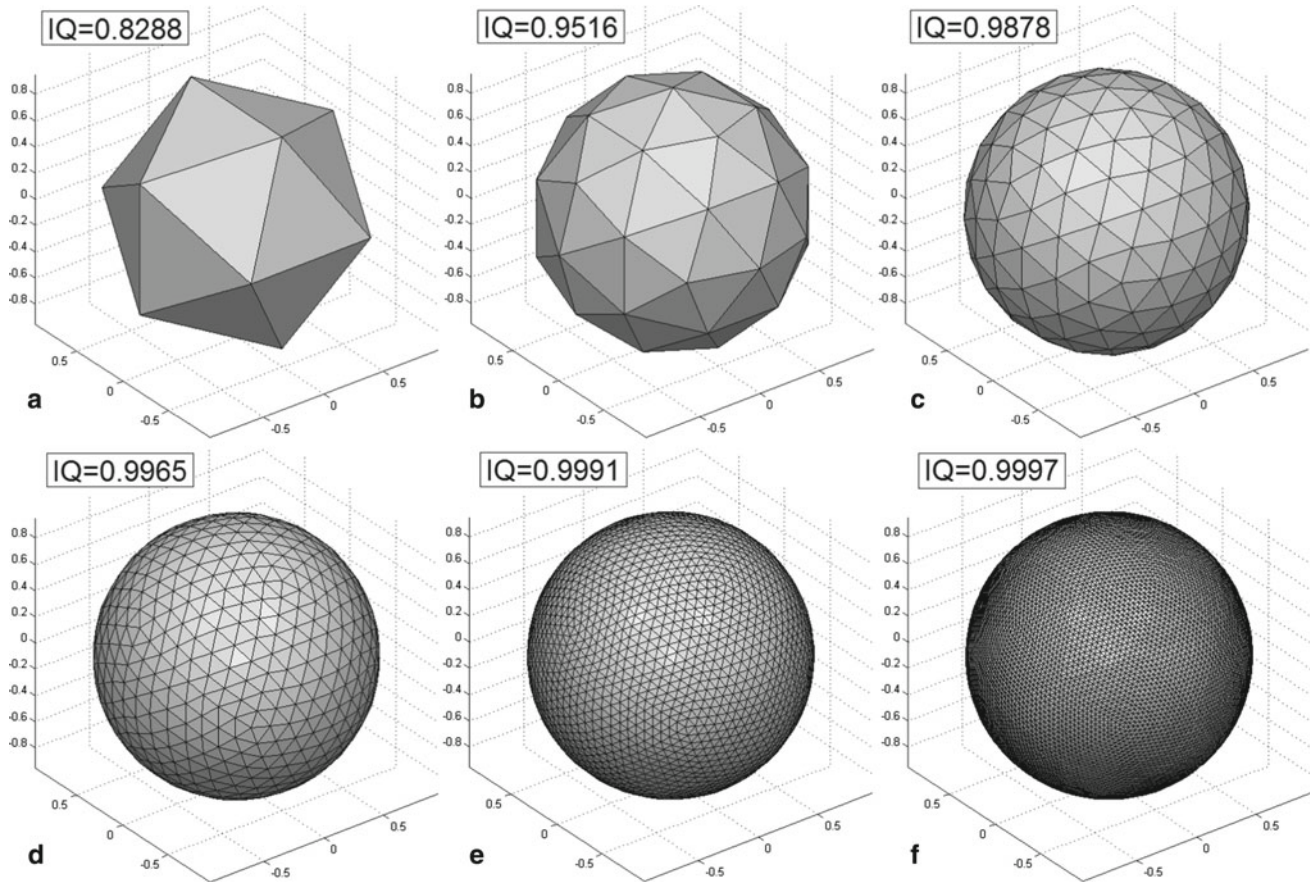

Fig. 3 Generation of geodesic structures. **a** Regular icosahedron (20 faces); **b–f** Geodesic structures of increasing complexities (respectively 80, 320, 1,280, 5,120 and 20,480 faces). The Isoperimetric Quotient (IQ) for each generation is given to illustrate the convergence towards the value IQ = 1 which corresponds to a perfect sphere

simple way. One simply has to consider the middle points of each of the 30 edges of the shape, and to project these middle points onto the circumscribed sphere of the solid. Then, each triangular facet is replaced by four facets (which are no longer coplanar), with all the vertices of the solid still lying on the sphere. This method is applied 5 times successively to define a solid composed of 10,242 vertices and 20,480 triangular facets (Fig. 3f). Such a polyhedron is a good approximation of a sphere (for example in terms of volume and of external surface) if the radial distance R of each point is kept constant, but can also be used to approximate any "star-like" shape by assigning a proper value of R to each of the 10,242 vertices. A given shape will thus be entirely defined by a collection $R_i\,(1 \leq i \leq 10242)$ of real positive numbers (the corresponding angles θ_i and φ_i being always the same as for the initial geodesic structure). This method will be used in conjunction with the 10,242 couples of angles so defined and the varying collections of radial distances to generate all the particle shapes presented in the sequel of this article. For the sake of simplicity, the radial distances will be called "radiuses" hereafter.

3.2 Cross sections

To generate random 3D surfaces, it may be interesting to consider first its three cross sections in the planes (x, y), (x, z), and (y, z) (Fig. 2c). Indeed, a complete method of generating random 2D contours has been proposed in [28] and was briefed in the previous section. In the present paper such 2D contours will be employed as a starting point for the generation of a 3D shape. As a demonstrative example, let us consider the three contours plotted in Fig. 4. Each of these contours was obtained using the Fourier spectrum of Toyoura sand which is well known in soil mechanics [33], with a random distribution of the phase angles. Each of these contours consists of 100 points defined in a local polar frame $r(\theta)$ with a subscript A, B, or C for each contour (Fig. 4a–c). In their current state, these 2D shapes cannot yet be considered as the three cross-sections of the same 3D shape in the three planes (x, y), (x, z), and (y, z), because some compatibility conditions are not fulfilled. Indeed, when projected onto their respective planes in space, these shapes should meet the following conditions along their common axis:

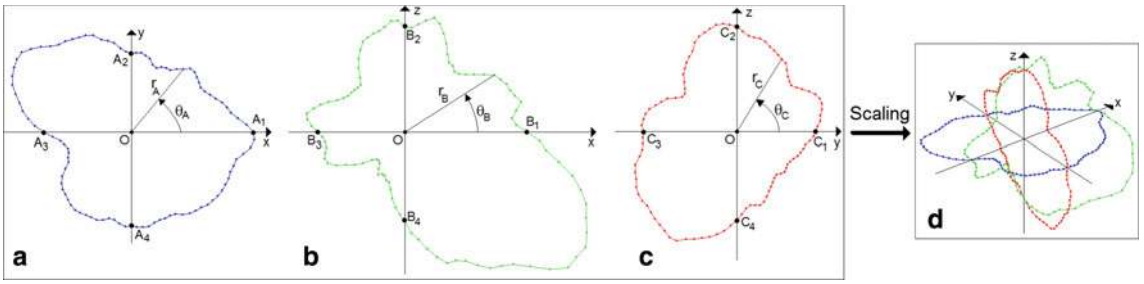

Fig. 4 Random 2D contours and their local systems of axis. **a** (x, y) plane; **b** (x, z) plane; **c** (y, z) plane; **d** scaled 2D contours in 3D space

$$OA_1 = OB_1 \quad \text{and} \quad OA_3 = OB_3 \quad (x \text{ axis}) \tag{10}$$

$$OA_2 = OC_1 \quad \text{and} \quad OA_4 = OC_3 \quad (y \text{ axis}) \tag{11}$$

$$OB_2 = OC_2 \quad \text{and} \quad OB_4 = OC_4 \quad (z \text{ axis}) \tag{12}$$

Obviously, these conditions are not fulfilled by the randomly generated contours, and a scaling process is necessary. Moreover, this scaling should be as smooth as possible to limit the disturbance to the contours, since we wish them to keep the features inherited from their original Fourier spectrum. A rather simple method is chosen here. The points A_1 to A_4 are kept unchanged, i.e. the (x, y) cross section is not modified (Fig. 4a). Then, the (x, z) contour is isotropically dilated (or contracted) to verify $OA_1 = OB_1$. This operation does not have any influence on the Fourier spectrum of the contour. However, to achieve the condition $OA_3 = OB_3$, a small modification of the shape is necessary. A correction of each radius (i.e. of each radial distance from O to one of the 100 points of the contour) is applied by multiplying it by a correcting factor δ_B which depends on the local angle θ_B (see Fig. 4b):

$$\begin{cases} \delta_B = 1 + \frac{\theta_B}{\pi} \cdot \frac{OA_3 - OB_3}{OB_3} & \text{if } 0 \le \theta_B \le \pi \\ \delta_B = 1 + \frac{2\pi - \theta_B}{\pi} \cdot \frac{OA_3 - OB_3}{OB_3} & \text{if } \pi \le \theta_B \le 2\pi \end{cases} \tag{13}$$

Such a correction is sufficient to verify Eq. (10). To further verify Eqs. (11) and (12), a similar correcting factor δ_C must be applied to each radius of the (y, z) contour as a function of the local angle θ_C, such that (Fig. 4c):

$$\begin{cases} \delta_C = \delta_1 + \frac{\theta_C}{\pi/2} \cdot (\delta_2 - \delta_1) & if\ 0 \le \theta_C \le \pi/2 \\ \delta_C = \delta_2 + \frac{\theta_C - \pi/2}{\pi/2} \cdot (\delta_3 - \delta_2) & if\ \pi/2 \le \theta_C \le \pi \\ \delta_C = \delta_3 + \frac{\theta_C - \pi}{\pi/2} \cdot (\delta_4 - \delta_3) & if\ \pi \le \theta_C \le 3\pi/2 \\ \delta_C = \delta_4 + \frac{\theta_C - 3\pi/2}{\pi/2} \cdot (\delta_1 - \delta_4) & if\ 3\pi/2 \le \theta_C \le 2\pi \end{cases} \tag{14}$$

where $\delta_1, \delta_2, \delta_3$, and δ_4 are the local correction factors at points C_1, C_2, C_3, and C_4, respectively:

$$\begin{cases} \delta_1 = OA_2/OC_1 \\ \delta_2 = OB_2/OC_2 \\ \delta_3 = OA_4/OC_3 \\ \delta_4 = OB_4/OC_4 \end{cases} \tag{15}$$

After these corrections, the three 2D contours are compatible and can be considered as the three cross-sections of the same solid (so far unspecified) in the 3D frame, as shown in Fig. 4d.

3.3 From the cross-sections to the solid particle

The scaling procedure described in the previous subsection is sufficient to generate three orthogonal cross sections of a hypothetic solid particle, but a generation of the complete 3D shape from these cross-sections is far from straightforward. Ideally, we wish any random cross section of the final solid particle to reflect the true features of a real particle as the three original cross-sections do in terms of frequencies and amplitudes of the irregularities, in order for these irregularities to be somehow "isotropically distributed" on the particle surface. Some kind of interpolation scheme is thus needed in order to reproduce these irregularities out of the planes (x, y), (x, z), and (y, z). An attempt to develop such a method is proposed hereafter, with its limitations being discussed at the end of this article.

The major schematic steps of this method are shown in Fig. 5, using the three cross sections described in the previous subsection (after scaling) as an example. We first consider the two cross-sections in the vertical planes (x, z) and (y, z) (Fig. 4b, c, respectively). Each of the two cross sections can be divided into two halves (located on either side of the z-axis), and each of these four half-sections can be used to generate a revolution solid (around the z-axis) as shown in Fig. 4d. Each of these solids actually corresponds to one of the four points A_1–A_4 (i.e. one of the four directions in the (x, y) system of axis). By analogy, they will be called solids S_1 to S_4, and defined by the radiuses $R_{1,i}(\theta_i, \varphi_i)$ to $R_{4,i}(\theta_i, \varphi_i)$ in the framework of the geodesic structure presented earlier (Fig. 5d). Since they are built by revolution, these radiuses R_i are independent on θ_i and are defined by:

$$\begin{cases} R_{1,i}(\theta_i, \varphi_i) = r_B(\theta_B) & \text{with} \quad \begin{cases} \theta_B = \pi/2 - \varphi_i & if\ \varphi_i \le \pi/2 \\ \theta_B = 5\pi/2 - \varphi_i & if\ \varphi_i \ge \pi/2 \end{cases} \\ R_{2,i}(\theta_i, \varphi_i) = r_C(\theta_C) & \text{with} \quad \begin{cases} \theta_C = \pi/2 - \varphi_i & if\ \varphi_i \le \pi/2 \\ \theta_C = 5\pi/2 - \varphi_i & if\ \varphi_i \ge \pi/2 \end{cases} \\ R_{3,i}(\theta_i, \varphi_i) = r_B(\theta_B) & \text{with} \quad \theta_B = \varphi_i + \pi/2 \\ R_{4,i}(\theta_i, \varphi_i) = r_C(\theta_C) & \text{with} \quad \theta_C = \varphi_i + \pi/2 \end{cases} \tag{16}$$

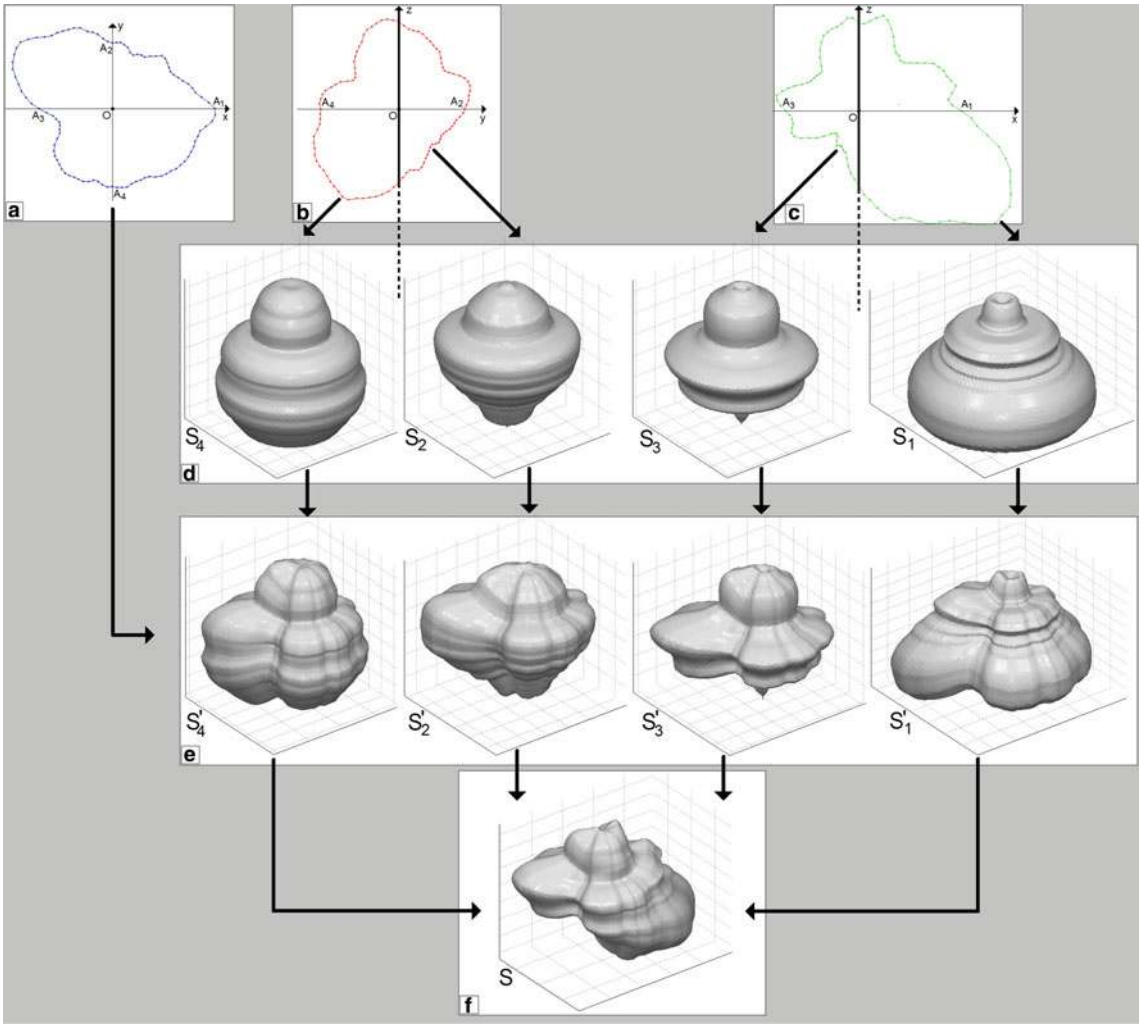

Fig. 5 Principle of the 3D generation method. **a** (x, y) cross-section; **b** (y, z) cross-section; **c** (x, z) cross-section; **d** solids S_1 to S_4 obtained by revolution of half-cross-sections; **e** solids S'_1 to S'_4 obtained by horizontal stretching of S_1 to S_4; **f** final solid S

These expressions are simple changes of the coordinate system from the local frames $(\mathrm{O}, r_\mathrm{B}, \theta_\mathrm{B})$ and $(\mathrm{O}, r_\mathrm{C}, \theta_\mathrm{C})$ to the global frame $(\mathrm{O}, R, \theta, \varphi)$.

The second step involves the generation of four new solids called S'_1 to S'_4, which are, respectively derived from S_1 to S_4 by somehow "stretching" them horizontally, accordingly to the horizontal cross-section previously defined in the plane (x, y) (Fig. 5a). Each of the solids S'_1 to S'_4 is thus defined by the collections of radiuses $R'_{1,i}(\theta_i, \varphi_i)$ to $R'_{4,i}(\theta_i, \varphi_i)$ (Fig. 5e) which are derived from $R_{1,i}(\theta_i, \varphi_i)$ to $R_{4,i}(\theta_i, \varphi_i)$ by the following expressions:

$$\left.\begin{aligned}
R'_{1,i}(\theta_i, \varphi_i) &= R_{1,i}(\theta_i, \varphi_i) \cdot \left[1 + \left(1 - \tfrac{|\varphi_i - \pi/2|}{\pi/2}\right) \cdot \tfrac{r_A(\theta_A) - r_A(0)}{r_A(0)}\right] \\
R'_{2,i}(\theta_i, \varphi_i) &= R_{2,i}(\theta_i, \varphi_i) \cdot \left[1 + \left(1 - \tfrac{|\varphi_i - \pi/2|}{\pi/2}\right) \cdot \tfrac{r_A(\theta_A) - r_A(\pi/2)}{r_A(\pi/2)}\right] \\
R'_{3,i}(\theta_i, \varphi_i) &= R_{3,i}(\theta_i, \varphi_i) \cdot \left[1 + \left(1 - \tfrac{|\varphi_i - \pi/2|}{\pi/2}\right) \cdot \tfrac{r_A(\theta_A) - r_A(\pi)}{r_A(\pi)}\right] \\
R'_{4,i}(\theta_i, \varphi_i) &= R_{4,i}(\theta_i, \varphi_i) \cdot \left[1 + \left(1 - \tfrac{|\varphi_i - \pi/2|}{\pi/2}\right) \cdot \tfrac{r_A(\theta_A) - r_A(3\pi/2)}{r_A(3\pi/2)}\right]
\end{aligned}\right\} \text{ with } \theta_A = \theta_i \tag{17}$$

The idea behind these equations is to multiply each radius R_i by a correcting term, in order for the equator ($\varphi_\mathrm{i} = \pi/2$) of the solid S' to match with the desired (x, y) cross-section, and meanwhile to keep the poles ($\varphi_\mathrm{i} = 0$ and $\varphi_\mathrm{i} = \pi$) undisturbed. Between these limits, the correction depends linearly on the angle φ_i.

The last step of the generation is the one leading to the final solid particle S defined by the collection of radiuses $R_i(\theta_i, \varphi_i)$, which are obtained by "morphing" among the four solids S'_1 to S'_4. This operation, being indeed a sort of

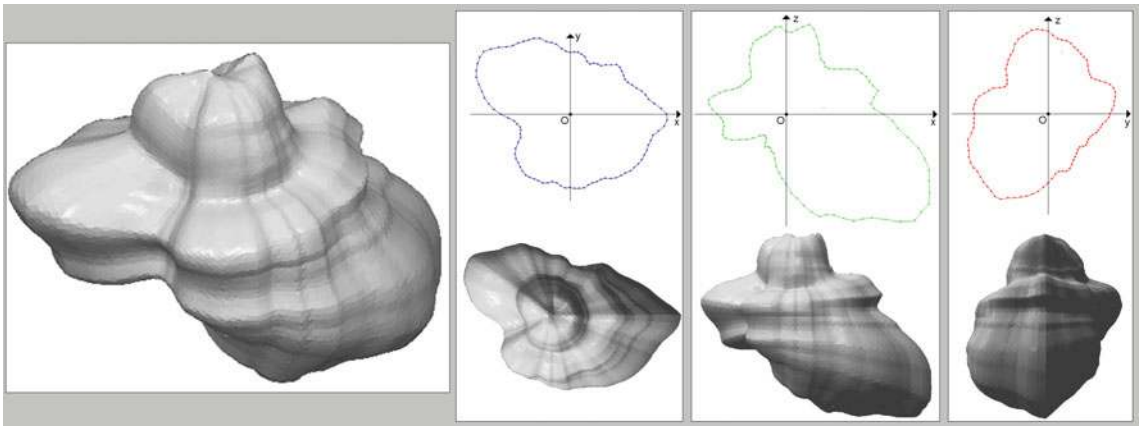

Fig. 6 Projection of the solid S on the three planes (x, y), (x, z), and (y, z), for comparison with the initial cross-sections

interpolation, is performed with respect to the angle θ, using the following expressions:

$$\begin{cases} R_i(\theta_i,\varphi_i) = R'_{1,i}(\theta_i,\varphi_i) + \dfrac{\left(R'_{2,i}(\theta_i,\varphi_i) - R'_{1,i}(\theta_i,\varphi_i)\right)}{\pi/2} \cdot \theta_i \;\; if \;\; 0 \le \theta_i \le \pi/2 \\ R_i(\theta_i,\varphi_i) = R'_{2,i}(\theta_i,\varphi_i) + \dfrac{\left(R'_{3,i}(\theta_i,\varphi_i) - R'_{2,i}(\theta_i,\varphi_i)\right)}{\pi/2} \cdot (\theta_i - \pi/2) \;\; if \;\; \pi/2 \le \theta_i \le \pi \\ R_i(\theta_i,\varphi_i) = R'_{3,i}(\theta_i,\varphi_i) + \dfrac{\left(R'_{4,i}(\theta_i,\varphi_i) - R'_{3,i}(\theta_i,\varphi_i)\right)}{\pi/2} \cdot (\theta_i - \pi) \;\; if \;\; \pi \le \theta_i \le 3\pi/2 \\ R_i(\theta_i,\varphi_i) = R'_{4,i}(\theta_i,\varphi_i) + \dfrac{\left(R'_{1,i}(\theta_i,\varphi_i) - R'_{4,i}(\theta_i,\varphi_i)\right)}{\pi/2} \cdot (\theta_i - 3\pi/2) \;\; if \;\; 3\pi/2 \le \theta_i \le 2\pi \end{cases} \tag{18}$$

The idea behind these expressions is fairly simple indeed. Each one of the four solids S'_1 to S'_4 is consistent with the target cross-sections on exactly one vertical half-profile, since each of them has been generated after operations on one half of an initial cross-sections. This is the reason why the final shape is interpolated in each $\pi/2$-interval of θ between the two solids which are relevant at the two limits of this interval (for example the two solids S'_2 and S'_3 on the interval $[\pi/2, \pi]$). The resulting solid S is presented in Fig. 5f. It can be clearly seen that its left part is similar to the one of S'_3 and its right part is similar to the one of S'_1, likewise for its front and back sides when compared to S'_2 and S'_4.

This generation method has been coded in a MATLAB 7 environment. The overall efficiency is reasonable, and the computational time is close to 5 s to generate a particle. Figure 6 provides a zoomed view of the solid particle S as well as its three projections onto the planes (x, y), (x, z), and (y, z). Evidently, these projections compare reasonably well with the three initial cross-sections that were used for the generation. The lack of perfect correspondence is related to the fact that they are projections rather than exact cross-sections, as will be entailed later in this paper. We note that the cross-sections of the solid particle S are actually *exactly* identical to the target ones.

4 Calibration of the generation method

As mentioned in the previous section, there is a small discrepancy between a given cross-section of a generated particle and the orthogonal projection of the particle on the same plane. This discrepancy is related to the fact that the particle under consideration may not be convex, and thus an orthogonal projection may be affected by certain irregularities which are "out of the plane" (not belonging to the cross-section). Meanwhile, the Fourier spectrums of sands available in the literature were invariably obtained from pictures of the sand grains, which may actually be considered as orthogonal projections of these grains if the focal length of the camera is long enough (this is indeed the case when the pictures are shot through microscopes, as is usually done for sand grains). Thus, the method proposed in this paper generates cross-sections of sand grains from Fourier spectrums that were actually obtained from orthogonal projections, and this fact may lead to inaccuracies if not properly accounted for.

To evaluate the influence of this discrepancy, we have considered the Fourier spectrums provided in [33] for six different sands (Fig. 7). These spectrums were obtained using a

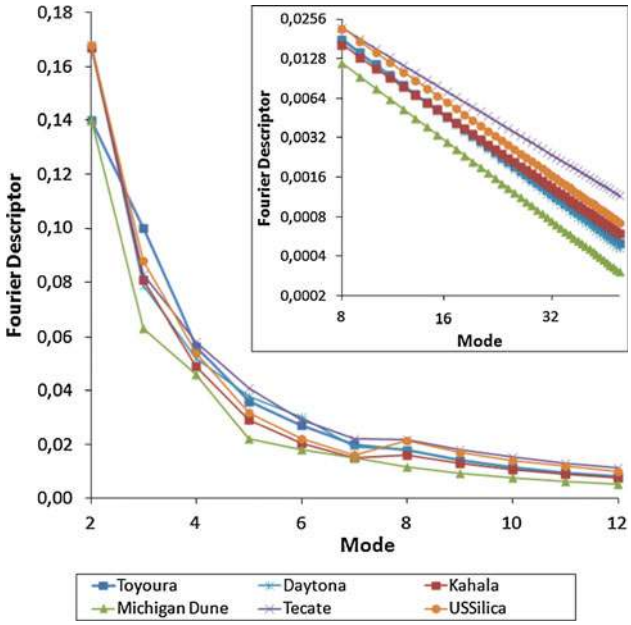

Fig. 7 Fourier spectrums provided by [33] for six sands; *Inset*: log2–log2 chart of the spectrums tails

semi-automatic procedure involving microscope photography and image treatment based on erosion-dilatation techniques as well as contrast enhancement. A good way to evaluate the accuracy of the proposed generation method is to reproduce numerically this experimental process. For each of the six sands, a total number of 1,000 virtual grains were generated using the method described in the previous section, based on the corresponding Fourier spectrums reported in [33]. Each of these generated particles was then subjected to a "virtual picturing", i.e. it was orthogonally projected in a random direction as shown in the two examples in Fig. 8. Finally, these 1,000 2D projections were used to compute the average Fourier spectrum for each sand reported in [33].

Figure 9 depicts the calculating results for two sands, Michigan Dune Sand and Tecate Beach Sand. The figure indicates that the measured spectrums of the generated particles are systematically smaller than the original ones that were used for the generations. The same trend has been found for the other four sands (Toyoura sand, Daytona sand, Kahala sand, and US Silica #1), though the results are not provided here. The trend implies that the generated grains are systematically more rounded and smoother than they should be, and that this error is indeed related to the discrepancy between the projections (used for the computation of spectrums, both experimentally and numerically) and the actual cross-sections (used for the particles generations). The process of orthogonal projection leads to a smoothing effect of the particle shape. The measured Fourier spectrums are hence affected by the smoothing and are not suitable to be used directly to generate the cross-sections. An appropriate correction of these input spectrums appears to be necessary to achieve more consistent results.

To calibrate this correction, the ratios $D_{n,cross}/D_{n,proj}$ between the input (i.e. cross-section-related as used in the generation process) and the measured (i.e. projection-related as obtained in the previous stage of "virtual photography") Fourier descriptors of the six sands are plotted in Fig. 10. The curves of these ratios with respect to the mode number suggest that the discrepancy between the projection-related and the cross-section-related spectrums follows some general trend. These ratios seem to be rather small (roughly 1.2) for the descriptor D_2 (which controls the particle elongation), and increase progressively for D_3 to D_8 (which control the main irregularities of the shapes), and reach a somehow constant value for the modes $D_n > 8$ (which control the surface roughness). This last observation is consistent with the results reported in the inserts of Fig. 9, which show that the input and measured spectrum (for modes larger than 8) follow some rather parallel evolutions in a log-log plot, suggesting a constant ratio between them.

Based on these observations, we propose the following general expression of correcting term α_n:

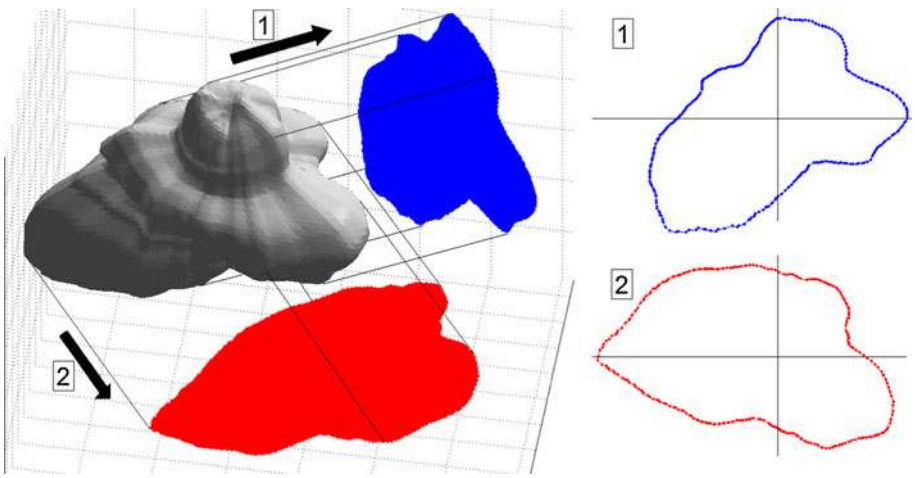

Fig. 8 Two examples of random orthogonal projection of the solid S, and the two corresponding 2D contours

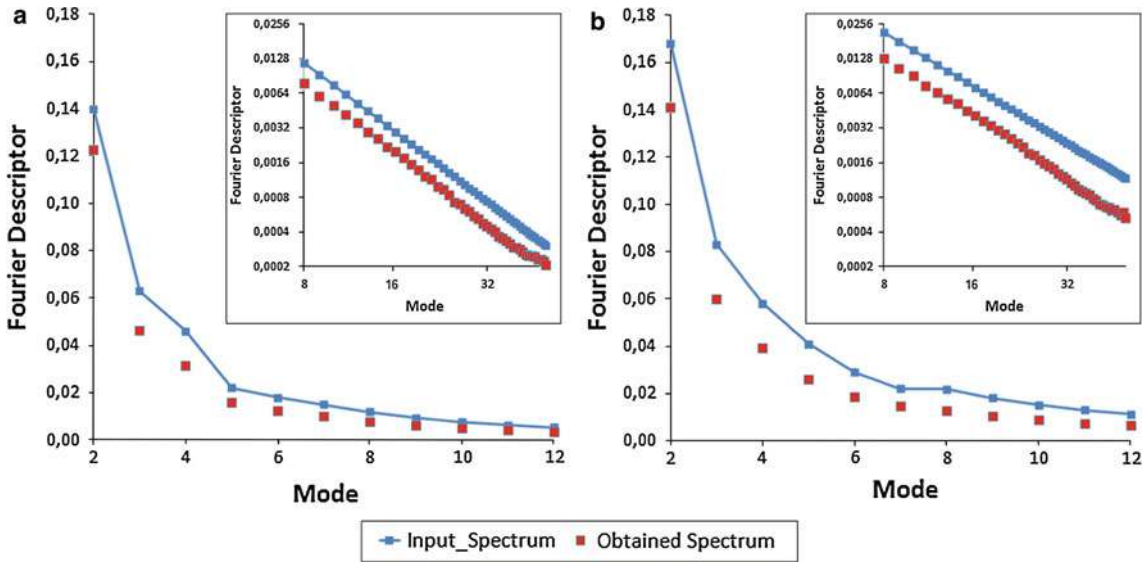

Fig. 9 Input spectrums (as provided by [33]) and obtained spectrums (as measured on the generated grains); **a** Michigan Dune sand; **b** Tecate River sand

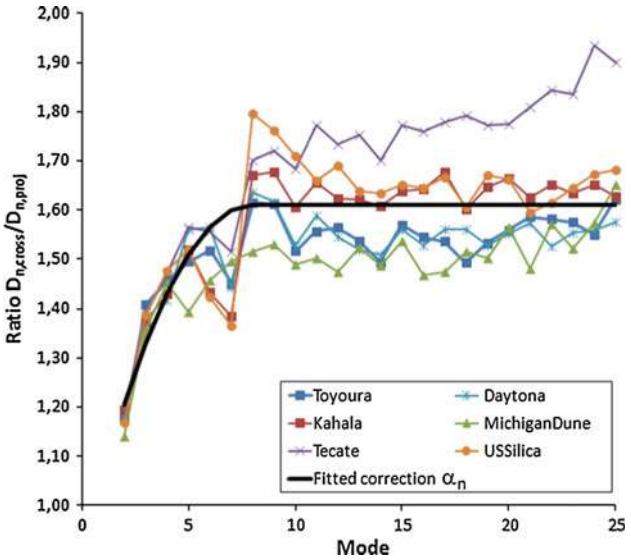

Fig. 10 Ratio $D_{n,cross}/D_{n,proj}$ between the input and obtained Fourier spectrums for the six tested sands, and fitted correcting term α_n

$$\begin{cases} \alpha_n = \left(\frac{\alpha_8-\alpha_2}{-36}\right)\cdot(n-2)^2 + \left(\frac{\alpha_8-\alpha_2}{3}\right)\cdot(n-2)+\alpha_2 \\ \quad for\ 2 \le n \le 8 \\ \alpha_n = \alpha_8\ for\ n \ge 8 \end{cases} \tag{19}$$

where n is the mode number, α_2 is the correcting term for $n = 2$, and α_8 is the correcting term for $n = 8$. For the six sands considered here, a mean-square-error fitting leads to the optimum parameters $\alpha_2 = 1.205$ and $\alpha_8 = 1.610$. The corresponding correction function α_n is plotted in Fig. 10. This correcting function appears to reconcile reasonably well the discrepancy between the input and the obtained spectrums, at least for the six sands on which it was fitted. Its general trend suggests that there are probably some hidden mechanisms which lead to the observation that the influence of the projection-process on the Fourier spectrum is smaller for the first number of modes and larger but constant for the modes larger than 8. The exact geometrical reason that gives rise to this observation still needs further investigations. Meanwhile, whether or not this fitted correcting function may be equally applied to other sands remains questionable, which demands further rigorous validations. The following section is devoted to this endeavor.

5 Validation of the proposed method

The corrected generation method described in Sect. 4 will be validated in this section. Three sands are considered here, namely, Michigan Beach sand, Niigata sand, and Ottawa sand. Note that none of them belongs to the six sands which have been considered in the calibration in last section. To our best knowledge, the present study is the first attempt on producing the Fourier spectrums for these sands. We nevertheless note that an interesting collection of grain photos of the three sands has been obtained by Scanning Electron Microscope (SEM) in [35] and [36]. An example of such a "micrograph" is presented in Fig. 11a for a grain of Michigan Beach sand [36]. As shown in Fig. 11, such a photo enables us to compute the Fourier spectrum of its contour. To this end, a semi-automatic MATLAB algorithm has been developed and employed to process the images (i.e. by converting the initial picture into a binary bitmap file with black pixels denoting the presence of matter and white pixels its absence, see Fig. 11b for example), to discretize the contour (by using a non-convex envelope algorithm presented in [19],

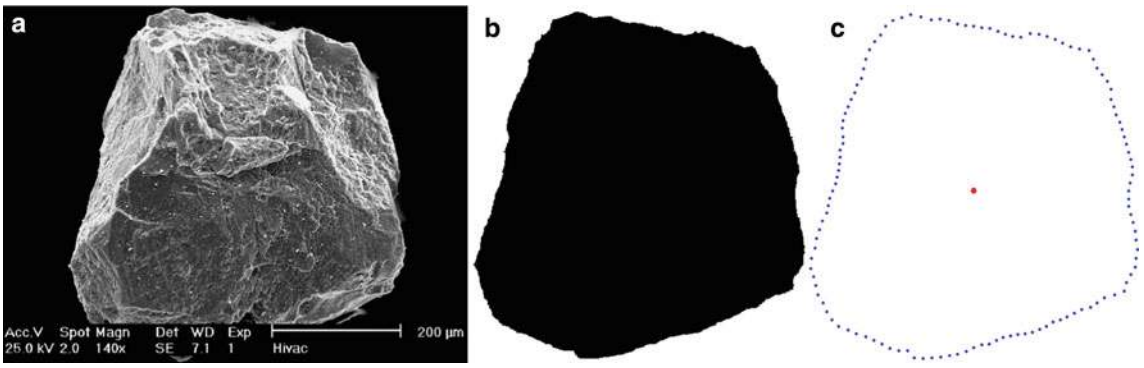

Fig. 11 Stages of experimental computation of Fourier spectrums. **a** A photo of sand grain obtained by scanning electron microscope (SEM) (from [36]), **b** image processing, **c** discretization of the non-convex envelope of the particle

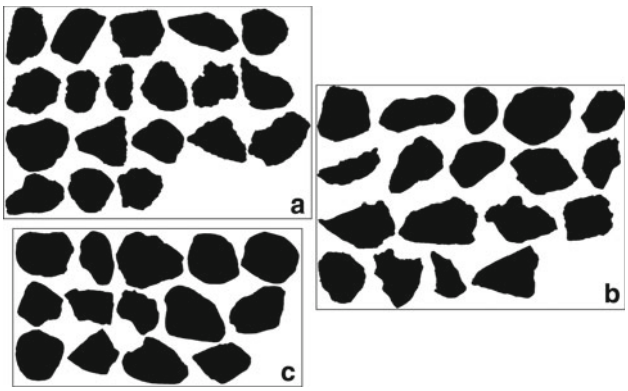

Fig. 12 Bitmap images obtained from all the processed SEM pictures. **a** Niigata sand (19 grains); **b** Michigan Beach sand (18 grains); **c** Ottawa sand (14 grains)

see Fig. 11c for demonstration), and finally to compute the discrete Fourier spectrum.

We take three sands reported in [35], namely, Michigan Beach sand, Niigata sand and Ottawa sand, to demonstrate the above validation process. These SEM photos of a total of 18 particles for Michigan Beach sand, 19 particles for Niigata sand and 14 for Ottawa sand are shown in Fig. 12 after treatment. Although limited, the database is considered statistically consistent and sufficient for our immediate purpose since it allows a satisfactory computation of the average Fourier descriptors D_{n} of each sand. The corrected spectrums D'_{n} are obtained by multiplication with the correcting term calibrated in the previous section:

$$D'_n = D_n \cdot \alpha_n \quad \forall n \geq 2 \tag{20}$$

These corrected spectrums D'_{n} are then introduced in the method presented in Sect. 3 to generate 1,000 virtual particles for each sand. As in the previous section, each of these particles is subjected to random orthogonal projections, and the average Fourier spectrum of 1,000 projected shapes is computed for the particle. The results of this validation process are plotted in Fig. 13 where the spectrums measured on the micrographs and calculated from the generated particles for the three sands are comparatively presented. Notably, the correspondence is fairly good for the three sands, both for the first modes ($2 \leq n \leq 8$) and for the spectrum tails ($n > 8$). This observation proves that the virtual particles generated by the proposed method can reproduce reasonably well the Fourier spectrums measured on pictures of real grains, and that the correcting term that was calibrated on six different sands may be considered as confidently satisfactory when applied to other sands.

6 Discussion and conclusion

To demonstrate the capacity of the proposed method, we further present in Fig. 14 the generated virtual particles in comparison with the real ones for Michigan Dune sand and Tecate River sand (Fig. 14a, b, respectively) reported in [33]. Four particles have been chosen for each sand to generate the virtual sands using their respective (corrected) spectrums. As shown in Fig. 14, the fundamental shape features of the real sand grains appear to be reproduced with a good accuracy by the proposed method. In particular, those shape features relevant to the Fourier spectrum have been reproduced well. Indeed, it was shown in [28] that this spectrum is able to quantitatively control at least four well-defined geometric descriptors of particles, namely, the elongation, the circularity, the roundness and the regularity. Since the method reproduces the Fourier spectrum of a grain well, so does it to these geometric descriptors. We are not sure, however, if the method may reproduce other descriptors which are not directly linked to the Fourier spectrums. Nevertheless, the proposed method appears to open up a door for a wide range of applications, by allowing the generation of realistic 3D particles to reproduce the major properties of sand and to introduce them in a DEM simulation of a sand assembly. Moreover, as shown in [28] in the 2D case, such a method offers flexible controls

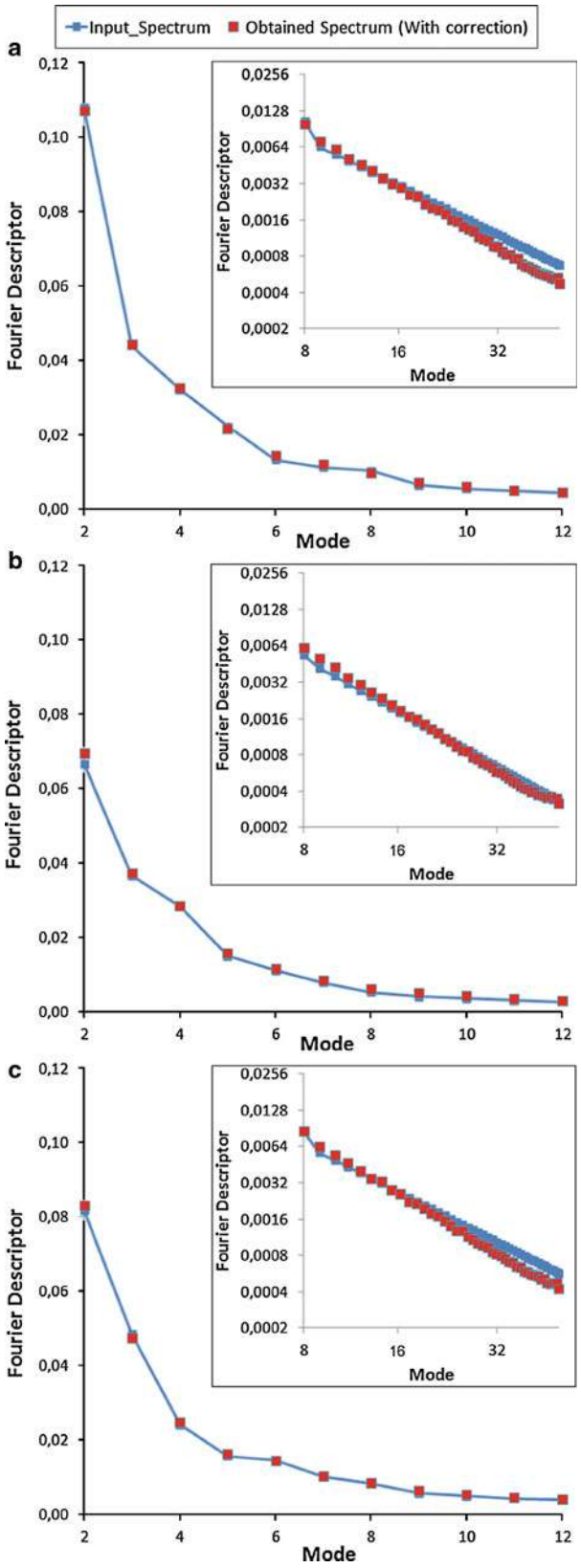

Fig. 13 Input spectrums (as computed from the pictures provided in [35]) and obtained spectrums (as measured on the grains generated with corrected spectrums). **a** Michigan Beach sand; **b** Ottawa sand; **c** Niigata sand

for us to tailor the input Fourier spectrums quantitatively to investigate the influence of a given shape descriptor (e.g. elongation or roundness) on the mechanical behavior of a granular material under specific conditions (shearing, flow, compaction, etc.). This proves to be useful for a variety of different engineering areas and industries dealing with granular particles of different nature.

Notwithstanding its merits, the current generation method does exhibit two minor drawbacks. The first one is directly related to the method used to create the 3D shape from the three cross-sections as explained in Sect. 3.3. Since this method is based on the shapes defined by the revolution of 2D profiles, we can observe in Fig. 14 a number of artifacts in the resulting 3D shapes. These artifacts are similar to holes and/or bumps that are aligned along specific directions, and form some kind of rifts and ridges in the vertical and horizontal directions. They are more visible on very irregular particles (such as the ones generated in Fig. 14b for the Tecate River sand, which is the one with the largest spectrum as shown in Fig. 7), and may lead to some limited "irregularity anisotropy". This shortcoming may be solved by developing a completely different generation method which would not involve any revolution of 2D profiles along an axis. This will be a focus of future work.

The second drawback can be clearly seen from Fig. 15. In this figure, two real grains of Niigata sand and Ottawa sand (Fig. 15a, b, respectively) are compared with four virtual grains generated with their corrected spectrums. The grains generated for Ottawa sand are expected to be more rounded than the ones for Niigata sand (since the spectrum of Ottawa sand is lower). Whilst a rough comparison of the generated grains with the real grains seems satisfactorily good, a closer inspection of the real sand grains reveals that they exhibit some "facets", i.e. some planar areas on certain parts of their surfaces bounded by sharp edges. Such property is not well reproduced by the generated grains. This is indeed an inherent drawback of using the Fourier spectrums to represent the surface configuration of a particle, regardless of its being in 2D or in 3D. This drawback is related to the loss of information induced by Eq. (1), as already mentioned before. Considering only the magnitudes of the Fourier modes but disregarding their phase angles is certainly problematic, because it is based on a presumption that these phase angles are statistically independent. This is obviously not always true, since the planar facets existing in real grains may actually correspond to some specific hidden structures and hence give rise to certain correlations in the phase angles of the Fourier modes. These features cannot be reproduced by a completely independent random generation as performed in the proposed generation method (Fig. 1b). Future work will be dedicated to finding a method of random sampling of the phase angles to reproduce such facets. Before this can be done, however, it is necessary to construct an indicator of this "facetted"

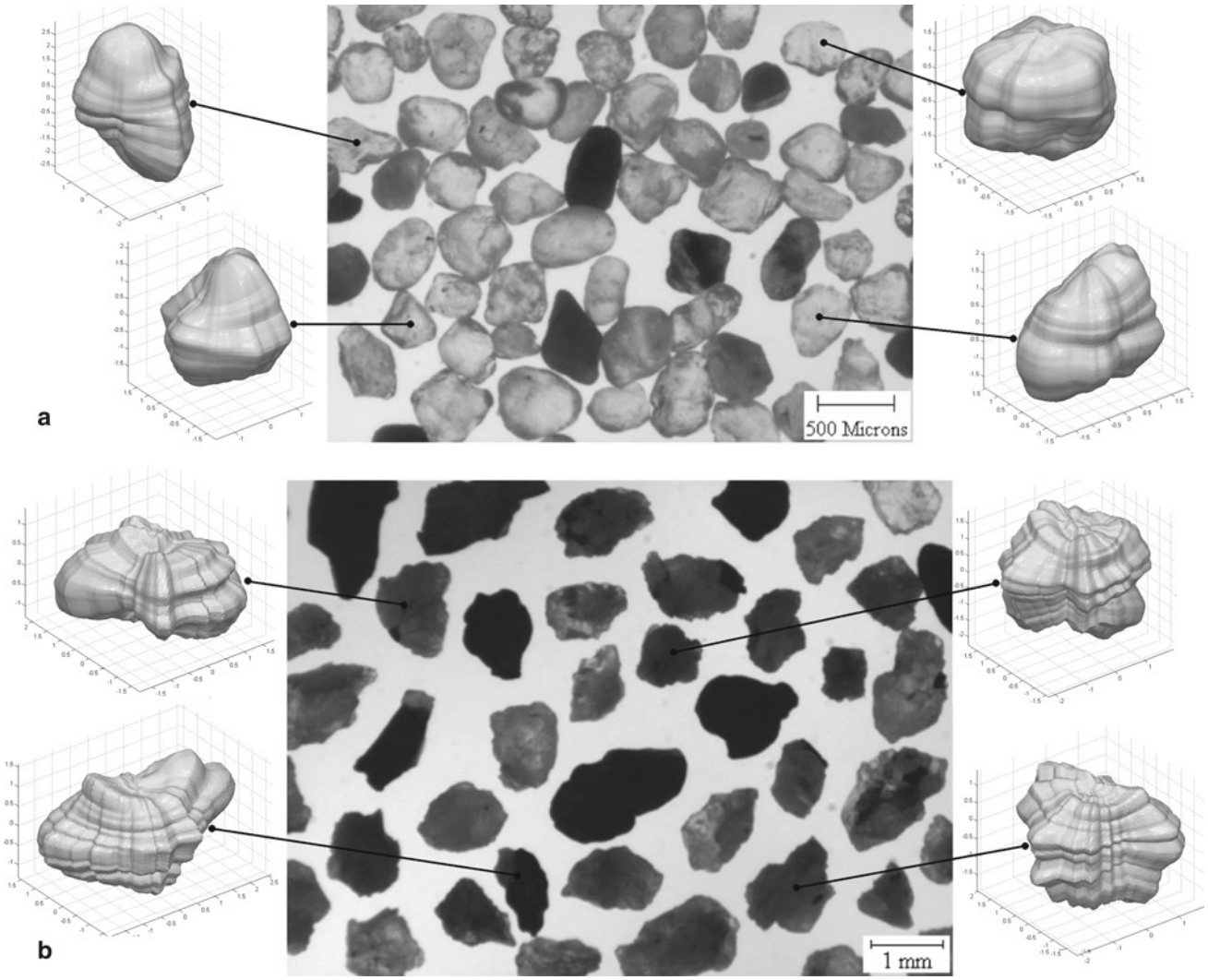

Fig. 14 Pictures of real sand samples (from [33]) and grains randomly generated with the relevant corrected Fourier spectrums (arrows are added to point out some fortuitous shape similarities, showing the benefit of the generation method). **a** Michigan Dune sand; **b** Tecate River sand

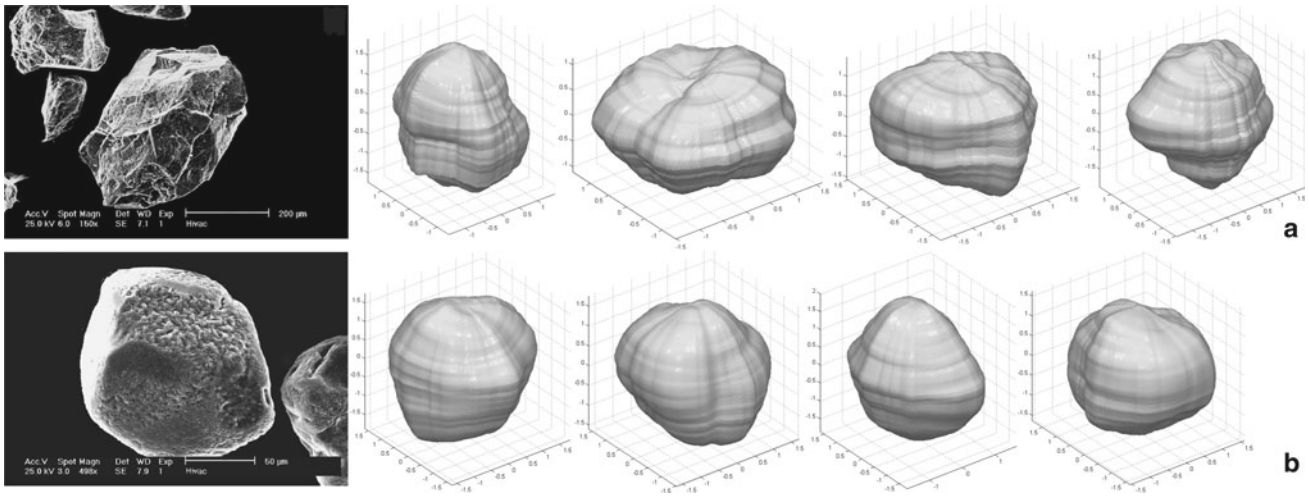

Fig. 15 SEM grain pictures (from [36]) and grains randomly generated with the relevant corrected Fourier spectrums. **a** Michigan Beach sand; **b** Ottawa sand

character for some particles which may allow a quantitative measurement of this visual property and can be used as a target value in an upgraded generation method in the future.

Other than addressing the above limitations, our future attention will be paid to the development of a technique (likely based on Constrained Voronoi Tessellation as in the 2D case described in [28]) to pack the generated 3D particles in a given container in an efficient manner, fulfilling some target values for certain quantities i.e., size distribution, void ratio/solid fraction and fabric anisotropy. Certain techniques are required to further introduce these complex shapes into a DEM code for practical simulations, such as the spheropolyedrons methodology and the Overlapping Discrete Element Clusters framework proposed in [37]. Meanwhile, it is also interesting to compare sand samples generated with this method with some real samples captured by more recent experimental works using advanced Micro Computed Tomography (μCT) or other modern apparatus (see, e.g., [38–40]).

Acknowledgments This work has been supported by Research Grants Council of Hong Kong through RGC/GRF 623609. The authors appreciate the comments provided by the two anonymous reviewers.

References

1. Taylor, D.W.: Fundamentals of Soil Mechanics. Wiley, New York (1948)
2. Mair, K., Frye, K.M., Maronez, C.: Influence of grain characteristics on the friction of granular shear zones. J. Geophys. Res. **107**(B10), 2219 (2002)
3. Damasceno, P.F., Engel, M., Glotzer, S.C.: Predictive self-assembly of polyhedra into complex structures. Science **337**, 453 (2012)
4. Cundall, P.A., Strack, O.D.L.: A discrete numerical model for granular assemblies. Geotechnique **29**, 47–65 (1979)
5. Thomas, P.A., Bray, J.D.: Capturing nonspherical shape of granular media with disk clusters. J. Geotech. Geoenviron. Eng. **125**, 169–178 (1999)
6. Jensen, R.P., Edil, T.B., Bosscher, P.J., Plesha, M.E., Ben Kahla, N.: Effect of particle shape on interface behavior of DEM-simulated granular materials. Int. J. Geomech. **1**(1), 1–19 (2001)
7. Salot, C., Gotteland, P., Villard, P.: Influence of relative density on granular materials behavior: DEM simulation of triaxial tests. Granul. Matter. **11**, 221–236 (2009)
8. Stahl, M., Konietzky, H.: Discrete element simulation of ballast and gravel under special consideration of grain-shape, grain-size and relative density. Granul. Matter. **13**, 417–428 (2011)
9. Katagiri, J., Matsushima, T., Yamada, Y.: Simple shear simulation of 3D irregularly-shaped particles by image-based DEM. Granul. Matter. **12**, 491–497 (2010)
10. Matsushima, T., Katagiri, J., Uesugi, K., Tsuchiyama, A., Nakano, T.: 3D shape characterization and image-based DEM simulation of the Lunar soil simulant FJS-1. J. Aerosp. Eng. **22**(1), 15–23 (2009)
11. McDowel, G., Li, H., Lowndes, I.: The importance of particle shape in discrete-element modelling of particle flow in a chute. Geotech. Lett. **1**(3), 59–64 (2011)
12. Tillemans, H.-J., Herrmann, H.-J.: Simulating deformations of granular solids under shear. Phys. A. **217**, 261–288 (1995a)
13. Pournin, L., Weber, M., Tsukahara, M., Ferrez, J.-A., Ramaioli, M., Liebling, ThM: Three-dimensional distinct element simulation of spherocylinder crystallization. Granul. Matter **7**(2–3), 119–126 (2005)
14. Azema, E., Radjai, F., Peyroux, R., Saussine, G.: Force transmission in a packing of pentagonal particles. Phys. Rev. E. **76**, 011301 (2007)
15. Azema, E., Radjai, F., Saussine, G.: Quasistatic rheology, force transmission and fabric properties of a packing of irregular polyhedral particles. Mech. Mater. **41**, 729–741 (2009)
16. Pena, A.A., Garcia-Rojo, R., Herrmann, H.J.: Influence of particle shape on sheared dense granular media. Granul. Matter **9**, 279–291 (2007)
17. Lu, M., McDowell, G.R.: The importance of modelling ballast particle shape in DEM. Granul. Matter **9**(1–2), 71–82 (2007)
18. Richefeu, V., Mollon, G., Daudon, D., Villard, P.: Dissipative contacts and realistic block shapes for modelling rock avalanches. Eng. Geol. **19**(150), 78–92 (2012). doi:10.1016/j.enggeo.2012.07.021
19. Mollon, G., Richefeu, V., Villard, P., Daudon, D.: Numerical simulation of rock avalanches: influence of a local dissipative contact model on the collective behavior of granular flows. J. Geophys. Res. Solid Earth AGU **117**, F02036 (2012). doi:10.1029/2011JF002202
20. Tillemans, H.-J., Herrmann, H.-J.: Simulating deformations of granular solids under shear. Phys. A. **217**, 261–288 (1995b)
21. Galindo-Torres, S.-A., Pedroso, D.-M.: Molecular dynamics simulations of complex-shaped particles using Voronoi-based spheropolyhedra. Phys. Rev. E. **81**, 061303 (2010)
22. Galindo-Torres, S.-A., Munoz, J.-D., Alonso-Marroquin, F.: Minkowski-Voronoi diagrams as a method to generate random packing of spheropolygons for the simulation of soils. Phys. Rev. E. **82**, 056713 (2010)
23. Ng, T.-T.: Particle shape effect on macro- and micro-behavior of monodisperse ellipsoids. Int. J. Numer. Anal. Methods Geomech. **33**, 511–527 (2009)
24. Ouadfel, H., Rothenburg, L.: "Stress-force fabric" relationship for assemblies of ellipsoids. Mech. Mater. **33**, 201–221 (2001)
25. Lin, X., Ng, T.T.: A three-dimensional discrete element model using arrays of ellipsoids. Géotechnique **47**(2), 319–329 (1997)
26. Azema, E., Radjai, F.: Stress-strain behavior and geometrical properties of packings of elongated particles. Phys. Rev. E. **81**, 051304 (2010)
27. Fu, P., Dafalias, Y.: Fabric evolution within shear bands of granular materials and its relation to critical state theory. Int. J. Numer. Anal. Methods Geomech. **35**(18), 1918–1948 (2011)
28. Mollon, G., Zhao, J.: Fourier–Voronoi-based generation of realistic samples for discrete modelling of granular materials. Granul. Matter **14**, 621–638 (2012). doi:10.1007/s10035-012-0356-x
29. Ehrlich, R., Weinberg, B.: An exact method for characterization of grain shape. J. Sediment. Petrol. **40**(1), 205–212 (1970)
30. Meloy, T.P.: Fast Fourier transform applied to shape analysis of particle silhouettes to obtain morphological data. Powder Technol. **17**, 27–35 (1977)
31. Bowman, E.T., Soga, K., Drummond, W.: Particle shape characterization using Fourier descriptor analysis. Geotechnique **51**(6), 545–554 (2001)
32. Garboczi, E.J.: Three-dimensional mathematical analysis of particle shape using X-ray tomography and spherical harmonics: application to aggregates used in concrete. Cem. Concret. Res. **32**(10), 1621–1638 (2002)
33. Das, N.: Modeling Three-Dimensional Shape of Sand Grains Using Discrete Element Method, p. 149. PhD Thesis. University of South Florida (2007)
34. Dobrohotoff, P.B., Imranullah, Azeezullah S.: Optimal description of two-dimensional complex-shaped objects using spheropolygons. Granul. Matter **14**, 651–658 (2012)

35. Vardhanabhuti, B.: The Coefficient of Eart Pressure at Rest and Deformation and Densification of Granular Soils Subjected to Static and Dynamic Loading, p. 1003. PhD Thesis. University of Illinois at Urbana-Champagn (2006)
36. Mesri, G., Vardhanabhuti, B.: Compression of granular materials. Can. Geotech. J. **46**, 369–392 (2009)
37. Ferellec, J.-F., McDowell, G.: A method to model realistic particle shape and inertia in DEM. Granul. Matter. **12**, 459–467 (2010)
38. Hall, S.A., Bornert, M., Desrues, J., Pannier, Y., Lenoir, N., Viggiani, G., Béuelle, P.: Discrete and continuum analysis of localised deformation in sand using X-ray μCT and volumetric digital image correlation. Géotechnique **60**(5), 315–322 (2010)
39. Hasan, A., Alshibli, K.: Three dimensional fabric evolution of sheared sand. Granul. Matter **14**, 469–482 (2012)
40. Ezaoui, A., Di Benedetto, H.: Experimental measurement of the global anisotropic elastic behaviour of dry Hostun sand during triaxial tests, and effect of sample preparation. Géotechnique **59**(7), 621–635 (2009)